Saturated tabletop x-ray laser system at 19 nm

Yuelin Li*

Institute of Laser Science and Applications, Lawrence Livermore National Laboratory, P.O. Box 808, Livermore, California 94550

James Dunn, Joseph Nilsen, Troy W. Barbee, Jr., and Albert L. Osterheld

Lawrence Livermore National Laboratory, P.O. Box 808, Livermore, California 94550

Vyacheslav N. Shlyaptsev

Department of Applied Science, University of California at Davis-Livermore, Livermore, California 94550

Received November 2, 1999; revised manuscript received January 6, 2000

Saturated operation of a tabletop x-ray laser at 19 nm is demonstrated with a laser-irradiated Mo slab target. The output energy, the intensity, the near-field beam pattern, and the beam divergence are characterized. The wavelength scalability and the high brightness make it a potential tool for x-ray laser applications.

OCIS codes: 140.3460, 140.7240, 140.7440, 350.5400.

1. INTRODUCTION

Among modern x-ray sources, x-ray lasers[1] have several distinct properties. Generated from plasma columns produced by lasers or other high-power machines, x-ray lasers deliver highly monochromatic x-ray emission with output energy up to millijoules with a bandwidth of $\Delta\lambda/\lambda \approx 0.01\%$ at wavelengths from 7 to 47 nm.[2–4] This has enabled applications such as microscopy of biological specimens[5] and probing of high-density plasmas,[6] relevant to laboratory astrophysics and inertial confinement fusion. However, so far these applications have been accomplished only with large laser facilities built for laser fusion research such as the Nova facility at Lawrence Livermore National Laboratory. The only saturated tabletop x-ray laser system is a capillary discharge,[3] which works at 47 nm and is difficult to scale to shorter wavelengths. For laser-pumped x-ray lasers, lasing in a relatively small-scale system has been demonstrated in Ne and Ni-like ions by use of ~30 J of pump energy by Tommasini and colleagues.[4]

We report the first saturated operation of a laser-pumped tabletop x-ray laser system using the novel transient-electron collisional excitation scheme with the wavelength ranging from 14 to 33 nm. The transient-electron collisional excitation scheme[7,8] uses a low-intensity, long laser pulse ($\sim 10^{12}$–$10^{13}\,\mathrm{W\,cm^{-2}}$, ~1 ns) to generate plasmas from solid targets, which is heated ~1 ns later by an intense, short laser pulse ($\sim 10^{15}\,\mathrm{W\,cm^{-2}}$, ~1 ps). The long pulse prepares properly ionized, large plasmas that allow better propagation of the x-ray laser beam and more efficient absorption of the short heating pulse. Kinetically, the ultrafast heating by the short, intense laser pulse generates unprecedented high gain and enables the x-ray laser to saturate with a small target length. Saturation of transient-electron collisional excitation x-ray lasers has been demonstrated previously with energy beyond the output of present tabletop lasers.[9]

2. EXPERIMENTAL SETUP

The saturated operation of the x-ray laser was demonstrated on the compact multipulse terawatt (COMET) laser system at Lawrence Livermore National Laboratory. The setup has been described before in detail.[10,11] Briefly, a long-pulse (~600-ps) and a short-pulse (~1-ps) beam from a tabletop, 1.053-μm Ti:sapphire–Nd:glass hybrid chirped-pulse amplification laser system are sent into the target chamber. The short pulse is focused onto the target to form an ~80 μm × 12.5 mm line focus, while the long pulse is two times broader to ensure a better overlap with the short pulse. The irradiances on the target surface are lower than 10^{12} and $10^{15}\,\mathrm{W\,cm^{-2}}$ for the long and the short pulses, respectively. The laser can be fired once every 4 min, and parameters including energy, pulse shape, pulse separation, near-field image, and spectrum were monitored. The line focuses were monitored with an x-ray slit camera coupled to a charge-coupled device (CCD).

To more efficiently use the short-lived (picosecond range) population inversion, we implemented a traveling-wave excitation setup using a five-segment stepped mirror.[12] A phase velocity of ~c toward the spectrometer was verified by a high-resolution optical streak-camera measurement.[13] We also did experiments to compare the x-ray laser output with and without the traveling wave. In the case without the traveling wave, the step mirror was simply replaced by a flat one.

We used both near-field imaging and spectroscopy methods to investigate the x-ray laser performance (Fig.

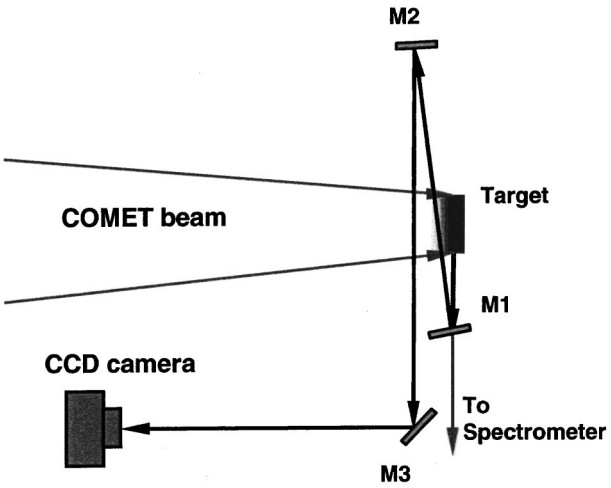

Fig. 1. Top view of the schematic setup for the x-ray laser experiment. The three multilayer x-ray mirrors M1 (spherical), M2 (planar), and M3 (planar) are used to image the output aperture of the x-ray laser onto the CCD with magnification of 14. The x-ray laser can be sent to the flat-field spectrometer with M1 translated out of its way.

1). Normally, the x-ray laser output is sent to an on-axis flat-field grating spectrometer coupled to a back-thinned CCD with a wavelength coverage of 14–35 nm. The spectrometer gives time-integrated spectra with angular resolution in the plane of the normal of the target and the axis of the line focus.

The imaging system (Fig. 1) consists of three Mo_2C/Si multilayer mirrors. One of them is spherical and images the output aperture of the x-ray laser onto a back-thinned x-ray CCD. The other two flat mirrors, one with normal and the other with 45° incidence, fold the beam to obtain a magnification of 14.1. With the 24-μm pixels of the CCD this gives a maximum spatial resolution of 1.7 μm. The calculated total reflectivity of the multilayer imaging system is 5.9% with a bandwidth of 1 nm at 18.9 nm. The narrow bandwidth of the system was verified by the absence of lasing signal for shots on Nb ($Z = 41$) and Ti ($Z = 22$) targets. To protect the multilayer mirrors from target debris and thereby attenuate the x-ray laser intensity and block the visible light, we used aluminum filters of a variety of attenuations.

3. RESULTS AND DISCUSSION

As has been demonstrated before,[14] using the traveling-wave geometry dramatically enhances the transient-gain x-ray laser output with respect to the case without the traveling wave. In Fig. 2 we compare the total output of the Ni-like $3d^9 4d^1 S_0 \rightarrow 3d^9 4p^1 P_1$ (here LS notation is used) in Mo at 18.9 nm as a function of delay between the long and the short pulses obtained from the imaging system (For a typical image, see Fig. 4). We obtain the relative output by subtracting the background plasma emission and by integrating the whole image. The traveling wave enhances the x-ray laser output by one to two orders of magnitude for delays of 0.1 to 0.9 ns. In addition, in the case with the traveling wave, the x-ray laser output is less sensitive to the change in delay. In the following, all results are obtained with the traveling wave.

The on-axis spectra are normally dominated by the Ni-like $3d^9 4d^1 S_0 \rightarrow 3d^9 4p^1 P_1$ laser line at 18.9 nm. There is a second weaker laser line at 22.6 nm, identified as the $3d^9 4f^1 P_1 \rightarrow 3d^9 4d^1 P_1$ transition[15] in Ni-like Mo [Fig. 3 (a)].

Saturation operation of the Ni-like Mo 18.9-nm x-ray laser is evidenced by its output as a function of the target length [Fig. 3(b)], which increases nonlinearly with the target length up to 8 mm and then becomes approximately linear afterwards. Fitting to the Linford

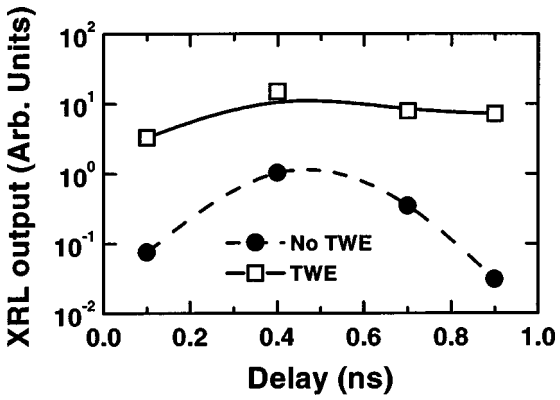

Fig. 2. Comparison of the total output of the Ni-like $3d^9 4d^1 S_0 \rightarrow 3d^9 4p^1 P_1$ in Mo at 18.9 nm as a function of delay between the long and the short pulses obtained from the imaging system with (TWE) and without the traveling wave (No TWE). The target length was 6 mm, with the long-pulse and short-pulse energy fixed at 0.8 J and 5 J.

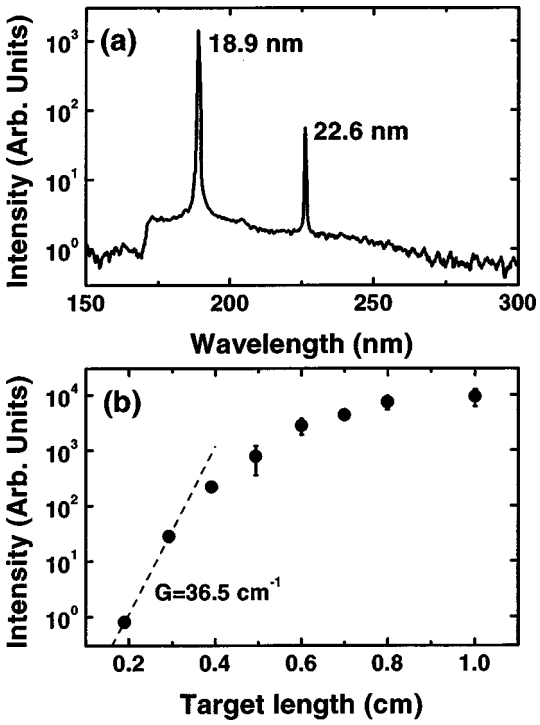

Fig. 3. (a) On-axis spectrum of the Ni-like Mo x-ray laser from a 10-mm-long target showing the Ni-like $4d^1 S_0 \rightarrow 4p^1 P_1$ and $4f^1 P_1 \rightarrow 4d^1 P_1$ lines at 18.9 and 22.6 nm, respectively. (b) The Ni-like Mo 18.9-nm x-ray laser output as a function of the target length with an overall gain–length product of 16.6. The long-pulse and short-pulse energies were 1.13 J and 5.02 J, respectively, with a delay of 0.7 ns. The error bars are due to fluctuations between shots.

formula[16] for each length and summing over the total target length, an overall gain–length product of ~16.6 is measured, 4.6 higher than that in a previous experiment without the traveling-wave excitation.[10,11] The main contribution is from the short target lengths, where a small signal gain of 36.5 cm^{-1} for up to 3-mm-long targets is measured, accounting for a gain length of ~11. As we were not able to measure the gain for targets shorter than 2 mm, which might be still higher, we believe the gain length is the lower limit on the error bar.

We notice that the gain coefficient falls continuously with increasing target length as in previous experiments,[9] starting at 36.5 cm^{-1} for 3-mm targets and decreasing to 5.6 cm^{-1} for 6- and 8-mm targets. We attribute this to two reasons. The first is the rapid spatial variation of the gain coefficients in combination with the beam refraction. The second is the transient gain lifetime in combination with the noncontinuous traveling wave. While the refraction deflects the x-ray laser beam from the high-gain, high-density region, the segmented traveling wave may not fully utilize the high gain with lifetime shorter than the segment length. Both effects deplete the effective gain at long target lengths.

A typical near-field pattern of the 18.9-nm x-ray laser is shown in Fig. 4, where the target surface is at $z = 0$ and the pump laser is incident from the top. The FWHM of the lasing region is 90 μm in the y direction (parallel to the target surface) and 70 μm in the z direction (normal to the target surface), with peak emission ~30 μm from the target surface. There are small-scale inhomogeneities, which may be caused by the different gain lengths experienced by the individual rays.

The imaging system also allows one to measure the absolute output energy of the x-ray laser. We did this by first subtracting the background plasma emission and then integrating the image and converting the CCD counts into the absolute energy using the CCD efficiency, the multilayer mirror reflectivity, and the filter transmission. The total output energy of the shot in Fig. 4 is 2.3 μJ. Taking into account the uncertainties in these parameters, we believe the measurement is the lower limit and that it could be a factor of 2 higher.

Saturated operation of the x-ray laser is also verified by the output intensity (Fig. 5), which we obtained by dividing the output energy with the area of the output aperture and an estimated pulse duration of ~7 ps. The estimate of pulse duration is based on the estimated gain duration of ~15 ps from the nontraveling-wave experiments where the gain lifetime is limiting the gain length.[11] Theoretically, considering spatial variation of the gain in the plasma, simulation with the LASNEX[17] and XRASER[18] kinetic codes estimated saturation intensities of 1.7–3.5 GW cm^{-2}. Comparing this with the measured x-ray laser intensity in Fig. 5, we found that the Ni-like Mo x-ray laser exceeds the saturation threshold in a large parameter space, evidencing the saturated operation and the robustness of the system. With a divergence of ~5 × 10 $mrad^2$, measured by the spectrometer, the Ni-like Mo x-ray laser brightness is found to be of the order of 10^{22}–10^{23} photons s^{-1} mm^{-2} $mrad^{-2}$ in a 0.01% bandwidth, 3 to 4 orders of magnitude higher than the brightest synchrotron sources at the same wavelengths. The

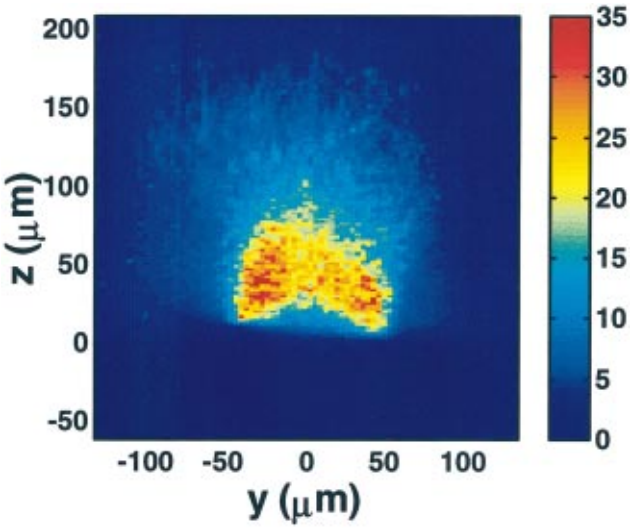

Fig. 4. Typical near-field image of the 18.9-nm Ni-like Mo x-ray laser for a 10-mm target. The target surface is at $z = 0$, and the pump laser is incident from the top. The energies in the long and short pulses are 3.94 J and 4.93 J, with a delay of 0.7 ns. The intensity is displayed in a unit of 10^3 CCD counts. 5300 counts per pixel correspond to an intensity of 1 GW cm^{-2}.

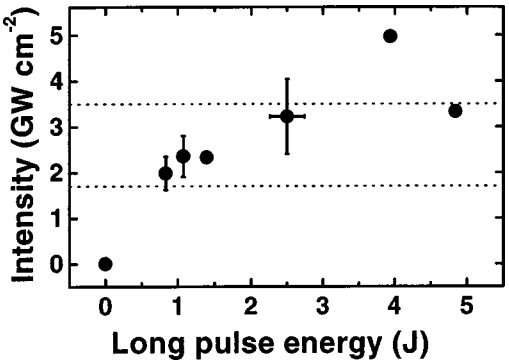

Fig. 5. 18.9-nm x-ray laser intensity at the output aperture as a function of the long-pulse energy at a delay of 0.7 ns and a constant short-pulse energy of 5 J. The target length is 1 cm. The dotted lines indicate the range of the theoretical saturation intensities.

reproducibility of the x-ray laser output energy and near-field pattern was also evidenced with the imaging system.

High output from Ni-like Zr to Cd, and Ne-like Ti to Fe, with wavelengths ranging from 14 nm to 33 nm, are also obtained. Such wavelength scalability is important for determining the chemical composition of specimens in biological and other applications.

4. CONCLUSION

In conclusion, we have demonstrated a saturated tabletop x-ray laser at 19 nm with output energy of up to 2.4 μJ with picosecond pulse duration and high brightness. Its robustness and scalability in photon energy, and especially the compactness, make it a very promising tool for x-ray applications.

ACKNOWLEDGMENTS

The authors thank M. Eckart, R. Ward, L. B. Da Silva, and H. Baldis for their support. We thank J. Hunter, B.

Sellick, H. Louis, and T. Demiris for technical support. The work was performed under the auspices of the U.S. Department of Energy by the Lawrence Livermore National Laboratory contract W-7405-Eng-48.

*Yuelin Li is currently at Argonne National Laboratory, Argonne, Illinois 60439.

REFERENCES

1. R. Elton, *X-Ray Lasers* (Academic, New York, 1990).
2. J. Zhang, A. G. MacPhee, J. Lin, E. Wolfrum, R. Smith, C. Danson, M. H. Key, C. L. S. Lewis, D. Neely, J. Nilsen, G. J. Pert, G. J. Tallents, and J. S. Wark, "A saturated X-ray laser beam at 7 nanometers," Science **276**, 1098 (1997).
3. C. D. Macchietto, B. R. Benware, and J. J. Rocca, "Generation of millijoule-level soft x-ray laser pulses at a 4-Hz repetition rate in a highly saturated tabletop capillary discharge amplifier," Opt. Lett. **24**, 1115–1117 (1999).
4. R. Tommasini, F. Lowenthal, and J. E. Balmer, "Saturation in a Ni-like Pd soft-x-ray laser at 14.7 nm," Phys. Rev. A **66**, 1577–1581 (1999); F. Lowenthal, R. Tommasini, and J. E. Balmer, "Observation of saturated lasing on the $3p-3s$, $J = 0-1$ transition at 25.5 nm in neon-like iron using a double-prepulse technique," Opt. Commun. **154**, 325 (1998).
5. L. B. Da Silva, J. E. Trebes, R. Balhorn, S. Mrowka, E. Anderson, D. T. Attwood, T. W. Barbee, Jr., J. Brase, M. Corzett, J. Gray, J. A. Koch, C. Lee, D. Kern, R. A. London, B. J. MacGowan, D. L. Matthews, and G. Stone, "X-ray laser microscopy of rat sperm nuclei," Science **258**, 269 (1992).
6. See R. Cauble, L. B. Da Silva, T. W. Barbee, Jr., P. Celliers, C. Decker, R. A. London, J. C. Moreno, J. E. Trebes, A. S. Wan, and F. Weber, "Simultaneous measurement of local gain and electron density in X-ray lasers," Science **273**, 1093 (1996), and references therein.
7. P. V. Nickles, V. N. Shlyaptsev, M. Kalachnikov, M. Schnürer, I. Will, and W. Sandner, "Short pulse X-ray laser at 32.6 nm based on transient gain in Ne-like titanium," Phys. Rev. Lett. **78**, 2748 (1997).
8. J. Dunn, A. L. Osterheld, R. Shepherd, W. E. White, V. N. Shlyaptsev, and R. E. Stewart, "Demonstration of X-ray amplification in transient gain nickel-like palladium scheme," Phys. Rev. Lett. **80**, 2825 (1998).
9. M. P. Kalachnikov, P. V. Nickles, M. Schnurer, W. Sandner, V. N. Shlyaptsev, C. Danson, D. Neely, E. Wolfrum, J. Zhang, A. Behjat, A. Demir, G. J. Tallents, P. J. Warwick, and C. L. S. Lewis, "Saturated operation of a transient collisional x-ray laser," Phys. Rev. A **57**, 4778 (1998); P. J. Warwick, C. L. S. Lewis, M. P. Kalachnikov, P. V. Nickles, M. Schnurer, A. Behjat, A. Demir, G. J. Tallents, D. Neely, E. Wolfrum, J. Zhang, and G. J. Pert, "Observation of high transient gain in the germanium x-ray laser at 19.6 nm," J. Opt. Soc. Am. B **15**, 1808–1814 (1998).
10. Y. L. Li, J. Nilsen, J. Dunn, A. L. Osterheld, A. Ryabtsev, and S. Churilov, "Wavelengths of the Ni-like $4d\,^1S_0 \rightarrow 4p\,^1P_1$ X-ray laser line," Phys. Rev. A **58**, R2668 (1998).
11. J. Dunn, J. Nilsen, A. L. Osterheld, Y. Li, and V. N. Shlyaptsev, "Demonstration of transient gain x-ray lasers near 20 nm for nickellike yttrium, zirconium, niobium, and molybdenum," Opt. Lett. **24**, 101–103 (1999).
12. J. R. Crespo Lopez-Urrutia, E. E. Fill, W. Theobald, and C. Wulker, "Travelling-wave excitation of an X-ray laser medium," Proc. SPIE **2012**, 258–264 (1994).
13. J. Dunn, Y. Li, A. L. Osterheld, J. Nilsen, S. J. Moon, and V. N. Shlyaptsev, "Table-top transient collisional excitation x-ray lasers" Proc. SPIE **3776**, 2–8 (1999).
14. A. Klisnick, D. Ros, P. Zeitoun, F. Albert, A. Carillon, P. Fourcade, S. Hubert, P. Jaeglé, G. Jamelot, C. L. S. Lewis, A. MacPhee, R. O'Rourke, R. Keenan, P. Nickles, K. Janulewicz, M. Kalashnikov, J. Warwick, J.-C. Chanteloup, E. Salmon, C. Sauteret, J. P. Zou, D. Joyeaux, and D. Phalippou, "Generation of intense Ni-like X-ray lasers at LULI: from 130 ps to 350 fs pumping pulses," Int. Phys. Conf. Ser. **159**, 107–114 (1999).
15. J. Nilsen, J. Dunn, A. L. Osterheld, and Y. L. Li, "Lasing on the self-photopumped nickel-like $4f\,^1P_1 \rightarrow 4d\,^1P_1$ X-ray transition," Phys. Rev. A **60**, R2677–R2680 (1999).
16. G. L. Linford, E. R. Peressini, W. R. Sooy, and M. L. Spaeth, "Very long lasers," Appl. Opt. **13**, 379–390 (1974).
17. G. B. Zimmermann and W. L. Kruer, "Numerical simulation of laser-initiated fusion," Comments Plasma Phys. Controlled Fusion **11**, 51–61 (1975).
18. J. Nilsen, "Radiative hydro modeling and atomic data bases," AIP Conf. Proc. **168**, 51–58 (1988).